

## Electrocatalytic Oxidation of Methanol on NiMnsalpnY Modified Glassy Carbon Electrode

Xia Hua<sup>1</sup>, Zhihong Gao<sup>1</sup>, Yan Wang<sup>1,\*</sup>, Wenyang Wang<sup>1</sup>, Baocheng Wang<sup>2</sup>, Ruifeng Li<sup>1,\*</sup>

<sup>1</sup> College of Chemistry and Chemical Engineering, Taiyuan University of Technology, Shanxi, 030024, China

<sup>2</sup> College of Materials Science and Engineering, Taiyuan University of Technology, Shanxi, 030024, China

\*E-mail: [wangyan@tyut.edu.cn](mailto:wangyan@tyut.edu.cn), [rfl@tyut.edu.cn](mailto:rfl@tyut.edu.cn)

Received: 28 February 2019/ Accepted: 26 April 2019 / Published: 30 June 2019

---

Zeolite composite catalyst NiMnsalpnY prepared by the flexible ligand method is examined for its redox process and electrocatalytic activities towards the oxidation of methanol. The methods of cyclic voltammetry (CV), chronoamperometry (CA), chronocoulometry (CC) and electrochemical impedance spectroscopy (EIS) are employed. The NiMnsalpnY composite system presents the characteristic of quasi-reversibility, which can be anticipated for the Ni(III)/Ni(II) couple. In the presence of methanol, the NiMnsalpnY modified electrode, compared with other modified electrodes, reveals a significantly higher response for the electrooxidation of methanol. The addition of a small amount of alloying element Mn to pure Ni can greatly enhance the ability of methanol electrooxidation. The anodic peak currents corresponding to methanol oxidation exhibit a linear dependency on the square root of the scan rate, indicating a diffusion controlled process. The electrocatalytic peak currents are proportional to the concentration of methanol, suggesting that the electrocatalytic oxidation of methanol at NiMnsalpnY/GC electrode seems to be certain. The mechanism of electrocatalytic methanol oxidation based on the electrochemical cyclic regeneration of Ni(III)Mn(III) active sites and their redox reaction with methanol in subsequent process is discussed. The kinetic parameters such as the electron transfer coefficient  $\alpha$  (the value is 0.34) of the electrode reaction, the diffusion coefficient  $D$  (the value is  $1.28 \times 10^{-8} \text{ cm}^2 \cdot \text{s}^{-1}$ ) of methanol and the catalytic rate constant  $k_{\text{cat}}$  (the value is  $1.55 \times 10^4 \text{ cm}^3 \cdot \text{mol}^{-1} \cdot \text{s}^{-1}$  for the concentration of 0.5M methanol) have been derived. The resistance of the electrocatalytic oxidation system has been investigated through the EIS regime.

---

**Keywords:** Zeolite, NiMnsalpnY, Methanol Electrooxidation, Zeolite Composite, Fuel Cell

### 1. INTRODUCTION

There is during the years increasing interest in the electrooxidation of methanol because of the development of direct methanol fuel cells (DMFC) as power sources for electronic devices [1-4]. The

DMFC is a promising future technology as an alternative to the conventional energy-generating devices, due to its high efficiency, very low pollution emissions, a potentially renewable fuel source, the ease of fuel storage and distribution, the fast and convenient refueling as well as the simple operation [5]. The low operation temperature of a DMFC (typically <math>95^{\circ}\text{C}</math>) allows for easy start up and rapid response to changes in load or operating conditions [6-8]. Nevertheless, one of the problems unsolved in the development of DMFCs is the slow kinetic of methanol oxidation on several electrode materials. Considerable efforts have been directed towards the study of methanol electrooxidation at high PH based on the assumption that electro-catalysis should be more facile in this alkaline medium [9, 10]. The use of alkaline solutions in a fuel cell has many advantages such as the increased efficiency [11], almost no sensitivity to surface structures [12], a wider selection of possible electrode materials and negligible poisoning effects in alkaline solution [13].

The electrode material is a distinctly crucial factor where a highly efficient electrocatalyst is needed in the electrochemical oxidation of methanol. Ni has commonly been used as an electrocatalyst for both anodic and cathodic reactions in the oxidation of alcohols [14, 15]. The addition of small amounts of alloying elements to Ni has shown a much improved electrochemical activity for the oxidation of methanol in alkaline media in comparison to the pure Ni electrode [16, 17]. This effect is motivated primarily from the anticipation of a synergistic electrocatalytic benefit from the combined properties of the components of alloys. Ni-Mn alloys have been used as important electrode materials because of their specific advantages such as lower poisoning effect, higher heat conductivity, greater electrocatalytic activity and stronger resistance to corrosion in alkaline media [18].

Zeolite-modified electrodes have been widely studied and applied in electrocatalysis over the past few years [19-22]. Zeolites, as the supporting materials for primary catalysts of methanol oxidation, are indispensable to produce the high catalytic activity. Zeolites with large surface area and porous structure are crucial to disperse catalyst particles and to reduce the catalyst loading under the condition of keeping high catalytic activity. A large number of articles have given an account of the preparation and the characterization of the transition metal Schiff-base complex modified zeolites [23-25]. The potential use of zeolite encapsulated metal complexes as heterogeneous redox catalysts is a promising area of research in redox catalysis [26-28]. It is predicted that the shape selectivity, electrostatics and acid-base properties of the zeolites are expected to synergistically enhance the reactivity of the physically entrapped complexes towards the redox reactions although the complexes will retain much of the original homogeneous catalytic properties [29]. Moreover, the complex encapsulated in the pores of zeolites have numerous advantages such as low mobility, high thermal stability, chemical stability and isolation from other molecules by the zeolite lattice [30-32].

In this work, the electrochemical behavior and the electrocatalytic oxidation of methanol at NiMnSalpnY/GC electrode in the alkaline solution have been studied by the methods of cyclic voltammetry, chronoamperometry, chronocoulometry and electrochemical impedance spectroscopy. It aims at the elucidation of the mechanism, the derivation of the kinetic parameters and the application of the electrocatalytic oxidation process.

## 2. EXPERIMENTAL

### 2.1 Reagent and apparatus

All chemicals and reagents used in this work were of analytical grade and used without further purification. 0.1M NaOH aqueous solution for electrochemical experiments was prepared using double distilled water. NaY was from the China Petroleum and Chemical Corporation and its ratio of SiO<sub>2</sub>/Al<sub>2</sub>O<sub>3</sub> is 5.6. Electrochemical measurements were carried out in a home-made one-compartment three electrode cell on a CHI model 600B (Shanghai, China) electrochemical workstation. Bare glassy carbon electrodes (GCEs, geometric area 0.0707cm<sup>2</sup>) and modified GCEs were used as the working electrodes. Pt plate (2mm×7mm) served as counter electrode and saturated calomel electrode (SCE) used as the reference electrode. High purity N<sub>2</sub> regulated by a flow-meter was used to maintain the deoxygenated environment in the measurement cell. All the experiments were performed at ambient temperature of 24±1°C.

### 2.2 Preparation of the NiMnY

NiMnY was prepared by ion-exchange method in a 0.01mol·L<sup>-1</sup> solution composed of Ni(CH<sub>3</sub>COO)<sub>2</sub> and Mn(CH<sub>3</sub>COO)<sub>2</sub> (the ratio of Ni/Mn is 9:1) at ambient temperature for three times (each time for 24h). Then, the solid fraction filtered out from the solution was washed twice with the deionized water and dried at 100°C for 12h. Encapsulation of metal complex was performed with the flexible ligand method [33]. First, NiMnY was intimately mixed with an excessive amount of Schiff-base ligands ( $n_{\text{ligand}}/n_{\text{metal}}=3$ ) in a crucible with cover. The complexation was carried out under high vacuum condition for 24h at the temperature of 130°C for H<sub>2</sub>salpn (H<sub>2</sub>salpn = *N,N'*-bis(salicylidene)-1,3-diaminopropane) [34]. Uncomplexed ligands that adsorbed on the exterior surface of the complex were removed by full Soxhlet extraction with acetone until the solvent was colorless. The extracted sample was ion-exchanged with 0.1M NaCl aqueous solution to be removed of the uncoordinated Ni<sup>2+</sup> and Mn<sup>2+</sup> before being washed with deionized water until no Cl<sup>-</sup> could be detected with AgNO<sub>3</sub> aqueous solution.

X-ray powder diffraction patterns were recorded on a Rigaku  $D_{\text{max}}/gA$  X-ray diffractometer with Cu  $K\alpha$  radiation. Fourier transform infrared (FT-IR) spectra were measured by a Perkin- Elmer 1600 FT-IR spectrometer using the conventional KBr pellet method. Before measuring, the sample was pretreated at 160°C for 6 h under high vacuum conditions. Field emission scanning electron microscopy (FE-SEM, S-4800II) was used to determine the crystallite size and morphology of the samples.

### 2.3 Preparation of modified electrode

Prior to each experiment, the glassy carbon electrodes were polished to a mirror-like surface with alumina and water slurry on a polishing cloth and rinsed with distilled water. Then, the GCEs were cleaned ultrasonically in acetone, absolute ethanol, HNO<sub>3</sub>-H<sub>2</sub>O (1:1, v/v) solution and double distilled water in the sequence in order to eliminate any trace of polishing paste from the surface, and then dried in the air before use.

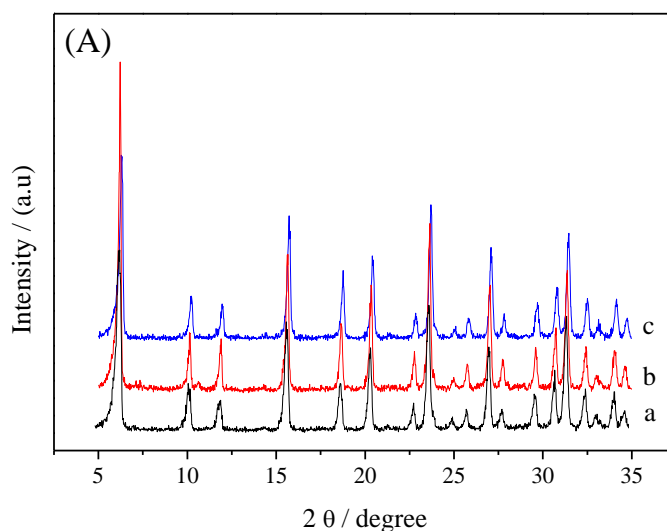
The modified electrodes were prepared through the procedure as described in the literature [35]. Typically, 30mg of NiMnsalpnY and 30mg of high purity graphite were dispersed in 1mL of tetrahydrofuran (THF) ultrasonically to form a suspension. Then, 3.5 $\mu$ L of this suspension was pipetted directly on the polished surface of the glassy carbon electrode and dried in the air at room temperature for approximately 1h. The modified electrode was further coated by 10 $\mu$ L of polystyrene solution in the THF solution and then dried overnight at room temperature. Thus, the NiMnsalpnY/GC modified electrode was obtained. The preparation process of other studied electrodes in this work such as NisalpnY/GCE, NiMnY/GCE, and graphite/GCE had the same procedure as that of NiMnsalpnY/GCE.

### 3. RESULTS AND DISCUSSION

#### 3.1. Characterization of NiMnsalpnY

XRD patterns of NaY, NiMnY and NiMnsalpnY are shown in Figure 1A. As can be seen, the peaks of the NiMnY and NiMnsalpnY samples both kept high correspondencewith the characteristics of the mesoporous zeolite NaY crystal structure. What's more, by comparison with mesoporous zeolite NaY, zeolitic host of NiMnsalpnY exhibited no obvious broadening of peak width and no distinct decreasing of relative intensity of the diffraction lines, demonstrating that the encapsulation of NiMn(salpn) in mesoporous zeolite Y by the flexible ligand method has no significant effect on the structure of zeolite Y.

IR spectra of NiMnY, NisalpnY, MnsalpnY and NiMnsalpnY are shown in Figure 1B. As can be seen, framework vibration bands attributed to mesoporous zeolite Y decided the spectra below 1200  $\text{cm}^{-1}$  for all samples. Otherwise, the bands from 1200 to 1600  $\text{cm}^{-1}$  attributed to aromatic ring and C=N vibrations of the salpn ligand could be clearly observed in the IR spectra of the NisalpnY, the MnsalpnY and the NiMnsalpnY samples.



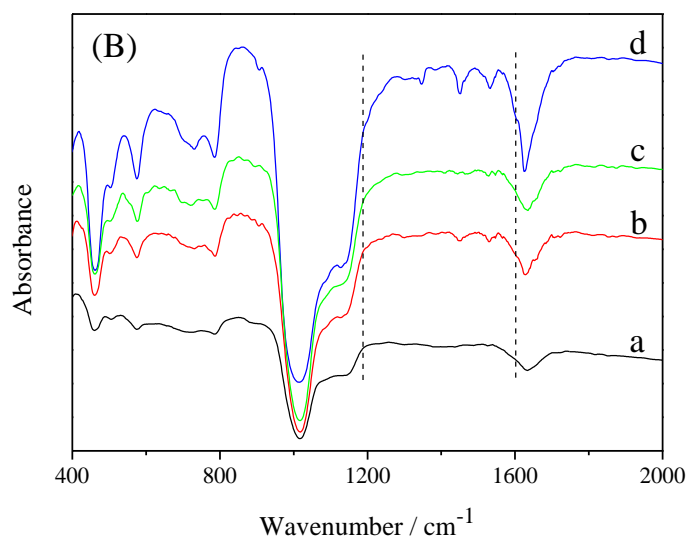


**Figure 1.** (A) X-ray diffractograms of (a) NaA, (b) NiMnY and (c) NiMnsalpnY samples. (B) FT-IR spectra of (a) NiMnY, (b) MnsalpnA, (c) NisalpnY and (d) NiMnsalpnY samples.

In contrast, these bands are absent in the spectra of the NiMnY. The ligand vibration bands in the other regions are substituted by the presence of zeolitic vibration bands. This indicates an effective evidence for the presence of transition metal complexes inside the cavity of zeolite Y in the NisalpnY, the MnsalpnY and the NiMnsalpnY samples.

Scanning electron microscopy (SEM) was conducted to analyze the surface structure of the samples. Figure 2 shows the micrographs recorded for the NiMnsalpnY (Figure 2A) and the NiMnsalpnY-graphite catalyst (Figure 2B). In Figure 2A, the sample of the NiMnsalpnY was round in shape with rugged surfaces. The sizes of the crystals were in the range of 700 to 1000 nm. On the other hand, Figure 2B shows the NiMnsalpnY at the electrode surface within the conducting graphite with NiMnsalpnY:graphite ratio of 1:1.

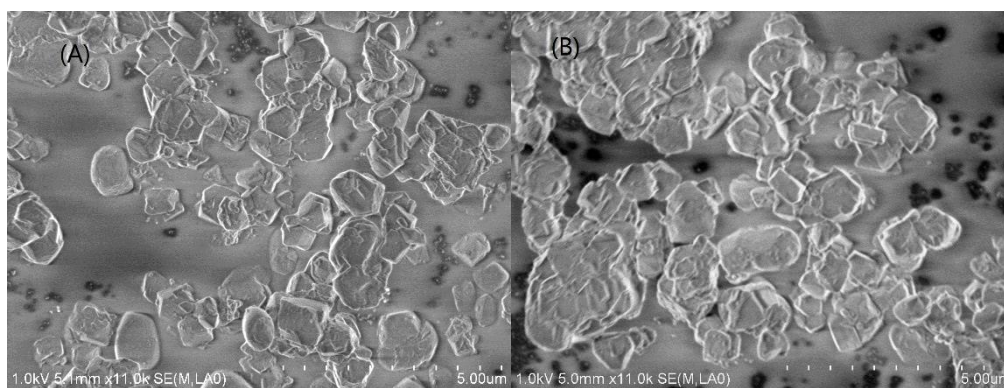


**Figure 2.** (A) Scanning electron micrograph of NiMnsalpnY. (B) Scanning electron micrograph of the NiMnsalpnY-graphite catalyst prepared with NiMnsalpnY:graphite ratios of 1:1.

Elemental analysis of NiMnsalpnY is given in Table 1. The elemental analyses of the sample revealed the presence of ligand with a C/N ratio roughly similar to that for neat complexes, and Ni:Mn molar ratios in NiMnsalpnY was almost close to 4. The NiMnsalpnY had M/N molar ratio of 1.03, which indicated that the total metal cations content and salpn ligands content were nearly equal to the stoichiometric requirement.

**Table 1.** Elemental analysis of the NiCosalenA catalyst.

Sample	C(wt%)	N(wt%)	Ni(wt%)	Mn(wt%)
NiMnsalpnY	6.74	0.93	1.18	0.32

### 3.2. Electrochemical behavior of NiMnsalpnY/GCE

Figure 3A presents the typical cyclic voltammograms of the electrochemical behavior of the NiMnsalpnY/GC electrode in 0.1MNaOH solution at different scan rates of 10-1500mV·s<sup>-1</sup>. As can be seen, the curves of CV reveal a nearly symmetric anodic and cathodic peaks which correspond to the Ni(III)/Ni(II) redox couple. As the scan rates increases, the difference value of the peak potential  $\Delta E_p(E_{pa}-E_{pc})$  increase gradually whereas the formal potential  $E^\circ(1/2(E_{pa}+E_{pc}))$  is almost equal to constant, suggesting that the electron transfer process of the chemical system should be quasi-reversible.

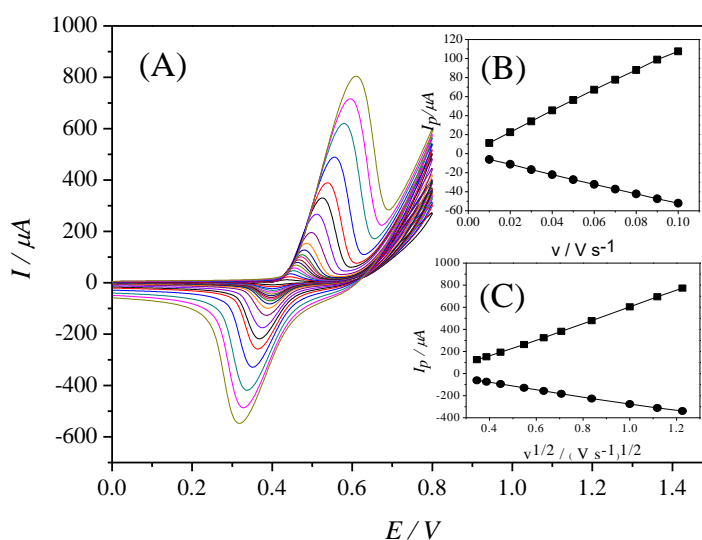


**Figure 3.** (A) Cyclic voltammograms of NiMnsalpnY/GCE in 0.1MNaOH solution at various scan rate (from inner to outer): 10, 20, 30, 40, 50, 60, 70, 80, 90, 100, 120, 150, 200, 300, 400, 500, 700, 1000, 1250, 1500mV·s<sup>-1</sup>. The inset B shows plots of anodic and cathodic peak currents versus the scan rate at lower values (10-100mV s<sup>-1</sup>). The inset C shows plots of anodic and cathodic peak currents versus the square root of scan rate at higher values (120-1500mV·s<sup>-1</sup>).

The peak currents are proportional to the scan rates in the range of 10-100mV·s<sup>-1</sup> (Inset B), indicating electrochemical activity of the surface confined redox process [36, 37]. Based on the slope of these two lines and using the equation, it follows that:

$$I_p = \frac{n^2 F^2 \nu A \Gamma_c}{4RT}$$

where  $I_p$  is the peak current,  $\Gamma_c$  is the surface coverage of the redox species,  $A$  is geometric area (approximate substitution of real area) of the electrode and the other symbols have their usual meanings. Taking the average of both the anodic and cathodic results, the value of  $\Gamma_c$  is calculated to be around  $1.198 \times 10^{-8} \text{ mol cm}^{-2}$ , corresponding to the amount of the electroactive ingredients of the NiMnsalpnY glassy carbon electrode. In the higher potential scan rates of  $120\text{--}1500 \text{ mV s}^{-1}$  (Inset C), the peak currents are linear dependency on the square root of scan rates, signifying the dominance of the surface species during the diffusion controlled process [38].

### 3.3. Electrocatalytic oxidation of methanol at NiMnsalpnY/GCE

Figure 4A displays the cyclic voltammograms of the electrocatalytic oxidation of methanol at NiMnsalpnY/GCE (curve d), NiMnY/GCE (curve c), pure graphite/GCE (curve b) and bare/GCE (curve a) in the presence of  $0.35 \text{ M}$  methanol in  $0.1 \text{ M NaOH}$  solution at the scan rate of  $10 \text{ mV s}^{-1}$ . The inset B shows the CVs of NiMnY/GCE and NiMnsalpnY/GCE in blank NaOH solution at the scan rate of  $50 \text{ mV s}^{-1}$ . The experimental results are derived based on the same amount of NiMn on the surface of various electrodes. As can be seen, the methanol oxidation at bare/GCE and pure graphite/GCE is very poor and it is impossible to get the oxidation peak.

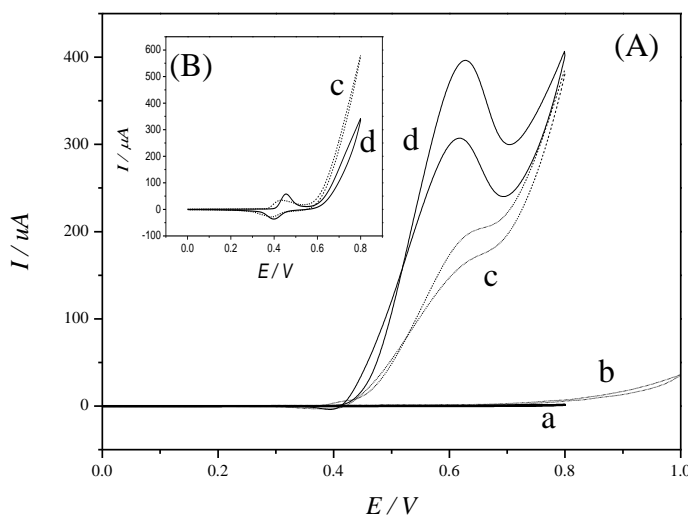


**Figure 4.** (A) Cyclic voltammograms of (a) bare/GCE, (b) graphite/GCE, (c) NiMnY/GCE, (d) NiMnsalpnY/GCE in  $0.1 \text{ M NaOH}$  solution in presence of  $0.35 \text{ M}$  methanol at the scan rate of  $10 \text{ mV s}^{-1}$ . The inset (B) shows CVs of (c) NiMnY/GCE and (d) NiMnsalpnY/GCE in  $0.1 \text{ M NaOH}$  solution in absence of methanol at the scan rate of  $50 \text{ mV s}^{-1}$ .

Nevertheless, at NiMnY/GCE and NiMnsalpnY/GCE the systems both exhibit an electrocatalytic activity towards the oxidation of methanol, but the electrocatalytic oxidation peak of NiMnsalpnY/GCE is more obvious and the peak current is much higher than that of NiMnY/GCE. These results clearly suggest that the NiMnsalpnY composite material modified electrode could significantly improve the

characteristic of methanol oxidation and it is the most active electrocatalyst among the four electrodes under study. The better electrocatalytic activity of NiMnsalpnY/GC electrode for methanol oxidation is attributed to the H<sub>2</sub>salpn ligand is N-donor ligand. The formation of complexes coordinated by N-donor ligand and the main catalyst (here pointing to Ni<sup>2+</sup> and Mn<sup>2+</sup>) can not only improve the catalytic activity and selectivity of the main catalyst, but also play an important role in corrosion inhibition [39].

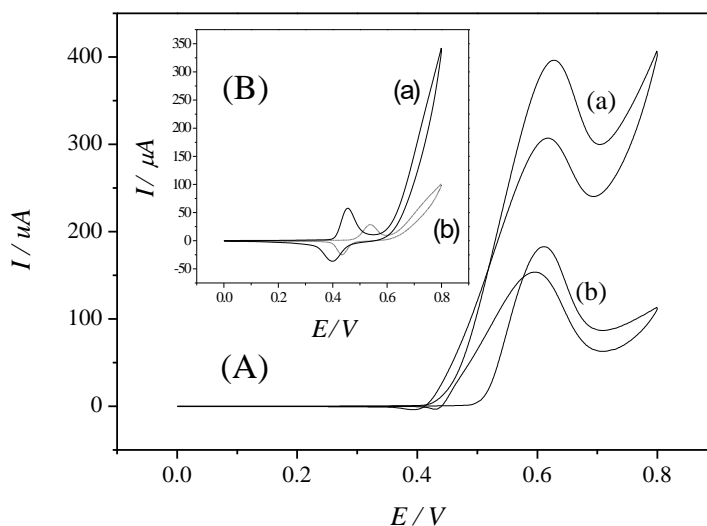


**Figure 5.** (A) Cyclic voltammograms of (a) NiMnsalpnY/GCE and (b) NisalpnY/GCE in 0.1M NaOH solution in presence of 0.35M methanol at the scan rate of  $10\text{mV}\cdot\text{s}^{-1}$ . The inset (B) displays CVs of (a) NiMnsalpnY/GCE and (b) NisalpnY/GCE in 0.1M NaOH solution in absence of methanol at the scan rate of  $50\text{mV}\cdot\text{s}^{-1}$ .

Figure 5A presents the cyclic voltammograms of NiMnsalpnY/GCE and NisalpnY/GCE in the presence of 0.35M methanol at the scan rate of  $10\text{mV}\cdot\text{s}^{-1}$ . The experimental results are obtained based on the same amount of NiMn on the surface of different electrodes. It is observed that the peak current density generated by NiMnsalpnY/GCE is higher than that generated by NisalpnY/GCE. Compared with that at NisalpnY/GCE, the larger response at NiMnsalpnY/GCE is estimated to be the result of the advanced adsorption of the methanol molecules at the Mn sites owing to a selected attraction through the non-bonded electron pairs of the O-atom of methanol inserting into the partially vacant d-orbital of the Mn species within the oxide film. The cyclic voltammograms of NiMnsalpnY/GCE and NisalpnY/GCE in the absence of methanol at the scan rate of  $50\text{mV}\cdot\text{s}^{-1}$  are shown in the inset B. The addition of the small amount of manganese in the alloy brings about the shift to the more negative potential values for the Ni(III)/Ni(II) couple. This shift is probably due to the overlapping of the waves of Ni(III)/Ni(II) and Mn(III)/Mn(II) couples and the increase of the charge-acceptance of Ni electrode [40]. The entire behavior is in accordance with the data reported previously in the literatures [41, 42].

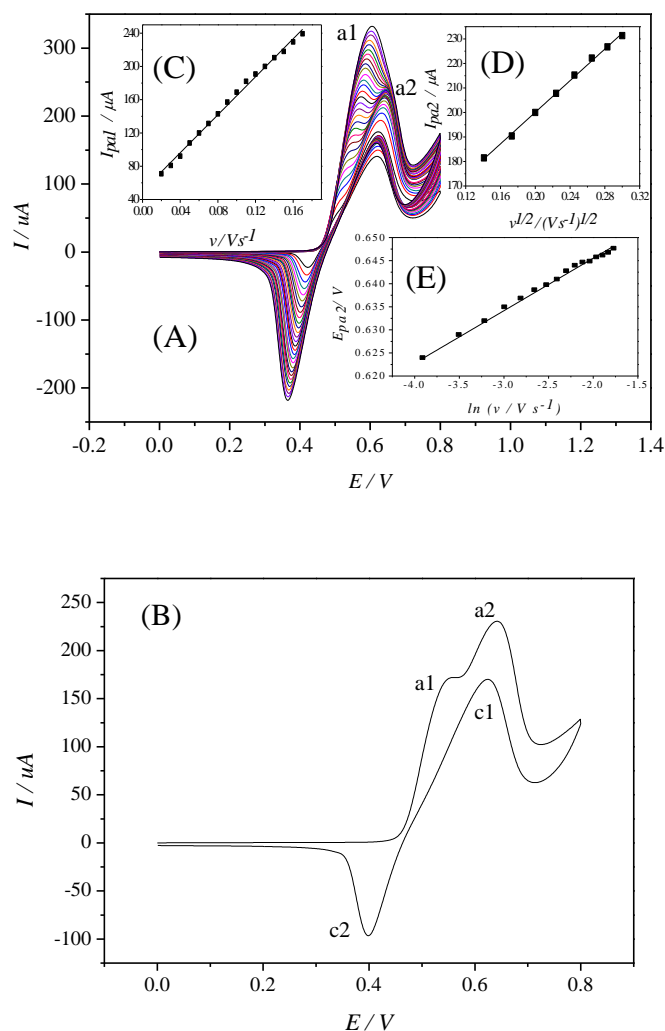


**Figure 6.** (A) Cyclic voltammograms of NiMnsalpnY/GCE in 0.1M NaOH solution containing 0.05M methanol at various scan rate (from inner to outer): 20-300  $\text{mV s}^{-1}$  (The interval is 10  $\text{mV}\cdot\text{s}^{-1}$ ). (B) Cyclic voltammograms at the scan rate of 100  $\text{mV s}^{-1}$  extracted from Figure 4 (A). The inset C shows plots of  $I_{pa1}$  versus the scan rate. The inset D shows plots of  $I_{pa2}$  versus the square root of scan rate at lower than 90  $\text{mV}\cdot\text{s}^{-1}$ . The inset E shows plots of  $E_{pa2}$  versus  $\ln v$  obtained from CVs.

**Table 2.** Comparisons of the peak potential ( $E_p$ ) and the peak current density ( $J$ ) reported for methanol electrooxidation on various Ni based electrodes.

Electrode	$E_p$ (V)	$J$ ( $\text{mA}/\text{cm}^2$ )	$v$ ( $\text{mV}/\text{s}$ )	Ref.
NiCo-CNFs	0.39	21.4	50	[43]
NiAl-LDH/GC	0.62	15.6	50	[44]
NiCu/GC	0.51	9.7	50	[45]
Ni-Co/GC	0.63	3.9	20	[46]
NP-NiCuP	0.35	3.6	10	[47]
NiCo/C-N/CNT	0.52	10.2	50	[48]
NiCu-G	0.53	10.6	50	[49]
NiMg-salen-zeolite A	0.47	5.3	50	[29]
NiMnsalpn/Y	0.62	4.2	20	This work
NiMnsalpn/Y	0.67	10.8	50	This work

<sup>a</sup>CNFs, carbon nanofibers, <sup>b</sup>LDH, layered double hydroxide, <sup>c</sup>NP, nano particle, <sup>d</sup>CNT, carbon nanotubes, <sup>e</sup>G, graphene, <sup>f</sup>salen, N, N'-bis(salicylidene)ethylenediamine, <sup>g</sup>salpn, N,N'-bis(salicylidene)-1,3-diaminopropane.

The electrocatalytic performance of NiMnsalpn/Y is listed in Table 2, including the peak potential and the peak current density. Moreover, different electrodes containing Ni used for methanol electrooxidation are also presented to make a comparison between the reported results and the outputs in this work. Clearly, this electrode composed of NiMn complex with salpn ligands coated in Y zeolite could exhibit favorable electrocatalytic activity on methanol oxidation, further serving as an efficient electrode material for methanol electrooxidation.

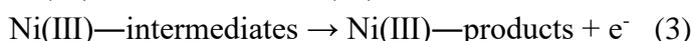
### 3.4. The effect of scan rate on electrocatalytic methanol oxidation at NiMnsalpnY/GCE

Cyclic voltammograms of NiMnsalpnY/GCE in the presence of 0.05M methanol in a 0.1M NaOH solution at various potential scan rates are illustrated in Figure 6A. In order to clarify the electrocatalytic mechanism of methanol oxidation at NiMnsalpnY/GCE, the 0.1M NaOH solution extracted cyclic voltammograms at the scan rate of 100mV s<sup>-1</sup> from main panel is shown in Figure 6B. It can be seen clearly from Figure 6B that electrocatalytic process takes place at four potential regions corresponding to the 0.1M NaOH solution four obvious peaks (a<sub>1</sub>, a<sub>2</sub>, c<sub>1</sub> and c<sub>2</sub>). In the first region, an anodic peak appearing at 0.553V (a<sub>1</sub>) signifies the oxidation from the Ni(II)Mn(II) to the Ni(III)Mn(III) species. Methanol molecules adsorbed on the Ni(III)Mn(III) active site surfaces are oxidized by direct electro-oxidation at higher potential corresponding to the peak a<sub>2</sub> [46]. In the later process, the number of active sites for methanol adsorption decreases and the intermediates and the products of the reaction produce a poisoning effect, tending to decrease the overall rate of methanol oxidation [50]. Thus, the anodic current passes through a maximum as the potential is anodically scanned. In the reverse half cycle, the Ni(III)Mn(III) active sites for the adsorption of methanol are regenerated by power source as a result of removing the intermediates and the products adsorbed on the Ni(III)Mn(III) active sites surface [51]. In consequence, the current goes through the maximum as the potential is cathodically scanned corresponding to the peak c<sub>1</sub>. In the end, a small cathodic peak c<sub>2</sub> turns up signifying that the active high valent metal species Ni(III) Mn(III) are reduced by methanol in the electrolyte solution.

Following, the mechanism of reaction process of the electrocatalyst NiMnsalpnY which is prepared by the complexation manner of congruent melting is represented. The actual ratio of Ni/Mn in NiMnsalpnY/GCE is got to be 4:1 by the method of elemental analysis. The redox transition of nickel species that presents in the electrocatalytic oxidation film is:



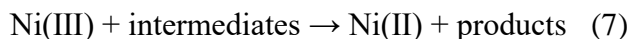
The adsorbed methanol is oxidized by direct electro-oxidation on the modified surface via the following reactions. The intermediate of the reaction process turns into carbocation. With further oxidation, the intermediate converts into methanol:



Ni(III) sites are regenerated by power source in the subsequent processes:



Ni(III) is reduced by methanol in the electrolyte solution in the end:



The products of reaction (6) and (7) (here pointing to Ni(II)) serve as the reactants of reaction (1). In this way, the reaction process of electrocatalytic oxidation goes on circularly.

Furthermore, it can be distinctly observed from the main panel of Figure 6A that the peak currents corresponding to the oxidation of metal species (peak  $a_1$ ) enhance obviously with the increasing scan rates and have a linear dependency on the scan rates as shown in Figure 6 (C), suggesting the surface confined redox process. The peak currents corresponding to the oxidation of methanol (peak  $a_2$ ) are linear proportional to the square root of the scan rates at lower scan rates than  $90\text{mV}\cdot\text{s}^{-1}$  as displayed in Figure 6D, indicating that the oxidation of methanol at the modified electrode is controlled by the diffusion of methanol from the solution to the surface redox sites [50]. At higher scan rates, the increment of the peak currents of methanol oxidation presents a decreasing tendency gradually and the peak  $a_2$  disappears completely at higher scan rates than  $300\text{mV}\cdot\text{s}^{-1}$ . This phenomenon indicates that the catalytic oxidation of methanol is much slower than the electrooxidation of metal species to higher valence state [45]. The oxidation of methanol on NiMn alloy may be a slow process. Thus, slow scan rates are suitable to obtain the high sensitivity or the low detection limits for the analytical purposes. Moreover, with the increasing potential scan rate the anodic peak potentials for both the peak  $a_1$  and the peak  $a_2$  shift to the positive potentials, while the cathodic peak potential for the peak  $c_2$  shifts to the negative potential. This result suggests that there is a kinetic limitation in the reaction between the redox sites Ni(III)Mn(III) and methanol. Figure 6E shows that the anodic peak potential for the peak  $a_2$  presents a linear dependency on the natural logarithm of the potential scan rate. For the irreversible-diffusion controlled reaction, the value of electron transfer coefficient can be obtained from the following equation [52]:

$$E_p = \left( \frac{RT}{n\alpha F} \right) \ln \nu + \text{constant}$$

where  $E_p$ ,  $\alpha$ , and  $\nu$  represent anodic peak potential, electron transfer coefficient and scan rate respectively. Using the slope of this line in Figure 6E, the value of  $\alpha$  is calculated to be 0.34. The data reveals a higher electron transfer rate compared with that of the pure Ni electrode ( $\alpha_{\text{Ni}}=0.16$ ) in the film of methanol electrooxidation.

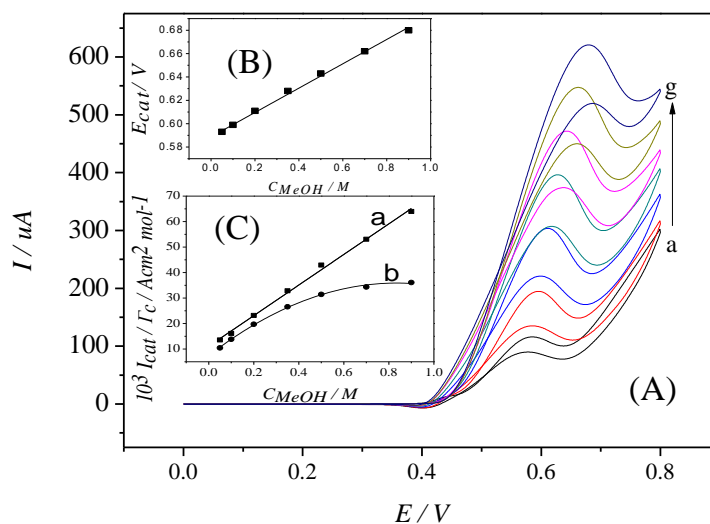


**Figure 7.** (A) Cyclic voltammograms of NiMnsalpnY/GCE in 0.1M NaOH solution in presence of (a) 0.05M, (b) 0.1M, (c) 0.2M, (d) 0.35M, (e) 0.5M, (f) 0.7M, (g) 0.9M of methanol at the scan rate of  $10\text{mV s}^{-1}$ . The inset B shows the plots of catalytic peak potential versus the concentration of methanol. The inset C shows the plots of catalytic peak currents normalized to the electrode surface coverage versus the concentration of methanol for (a) NiMnsalpnY/GCE and (b) NisalpnY/GCE.

### 3.5. Effect of methanol concentration

The cyclic voltammograms of NiMnsalpnY/GC electrode in the presence of various concentration of methanol (0.05M-0.9M) in a 0.1M NaOH solution at a potential scan rate of  $10\text{mV s}^{-1}$  are displayed in Figure 7 A. As can be seen, the electrocatalytic peak presents a positive shift in the peak potential, and the peak potential is linear dependency on the concentration of methanol as shown in the inset B. The electrocatalytic peak currents increase obviously, which are followed by the decreasing cathodic peak currents with the increasing concentration of methanol. The decreasing cathodic currents ensue the oxidation process in the reverse cycle indicate the incapability of reducing the entire high valent metal species formed in the oxidation cycle and that the rate determining step certainly involves the effect of methanol. The inset (C) demonstrates a correlation between the electrocatalytic peak currents normalized to the electrode surface coverage and the concentration of methanol. The curve a and curve b represent NiMnsalpnY/GCE and NisalpnY/GCE respectively. As can be observed, the electrocatalytic peak currents generated by the NiMnsalpnY/GC electrode are linear proportional to the concentration of methanol. The detection limit is  $281.54\text{mM}$  ( $3\sigma/s$ , where  $\sigma$  is the standard deviation of the intercept and  $s$  is the slope of curve a [53]). It implies that any increase in the concentration of methanol brings about an almost proportional linear enhancement of the electrocatalytic currents. That is to say, electrocatalytic oxidation of methanol at the NiMnsalpnY/GC electrode seems to be certain. However, at the NisalpnY/GC electrode, the electrocatalytic currents are proportional to the methanol concentration below 0.35M. At a higher concentration, probably all the Ni(III) catalytic active sites are saturated and then the value of peak currents tends to be constant. This phenomenon indicates that the

addition of small amounts of alloying element Mn to Ni can significantly enhance the ability of methanol electrooxidation in comparison to the pure Ni-based electrode, which is due to the synergistic electrocatalytic effect from the combined properties of the Ni and Mn of alloys.

### 3.6. Chronoamperometric studies

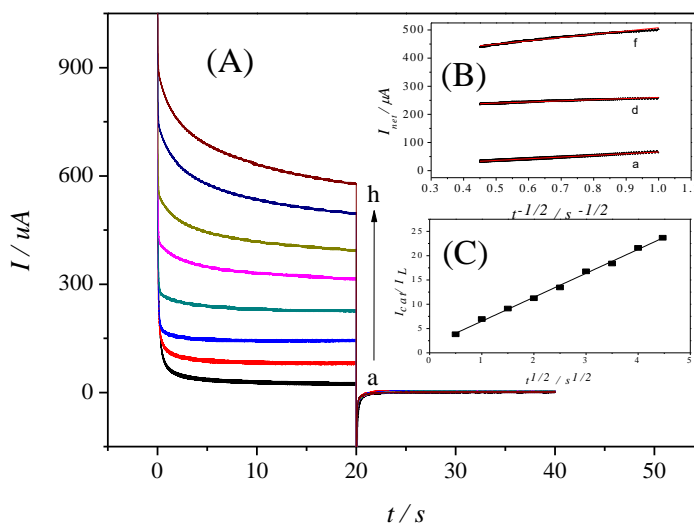


**Figure 8.** (A) Chronoamperogram of NiMnSalpnY/GC electrode in absence (a) and presence various concentration of methanol in the range of 0.05M-0.9M (b-h). Potential steps were 660 and 300mV, respectively. (B) Dependency of net current on  $t^{-1/2}$  for (a) 0M, (d) 0.2M, (f) 0.5M methanol. (C) Dependency of  $I_{\text{cat}}/I_L$  on  $t^{1/2}$  for 0.5M methanol.

Chronoamperometry is employed for the investigation of the kinetics of electro-catalytic oxidation of methanol at the NiMnSalpnY/GC electrode. The catalytic rate constant as well as the diffusion coefficient of methanol can be evaluated from the chronoamperometric regime. Figure 8A presents the double step chronoamperograms for NiMnSalpnY/GCE in the absence (a) and presence (b-h) of various concentration of methanol with applied potential steps of 660mV and 300mV, respectively. The forward currents increase gradually with the increasing concentration of methanol, while the backward currents are negligible when the potential is stepped down to 300mV. The result indicates that methanol oxidation is an irreversible process [38]. Figure 8B shows the net current is linear dependent on the inverse of the square root of time. The net current is determined by the point-to-point subtraction of the forward current found for the bare glassy carbon electrode from that for the NiMnSalpnY/GCE in the presence and absence of methanol. The process of methanol oxidation accords with the near Cottrellian behavior which can be explained by the diffusion-controlled process in the film [54]. The value of diffusion coefficient is determined by the Cottrell equation:

$$I_{\text{net}} = nFAD^{1/2}c\pi^{-1/2}t^{-1/2}$$

where  $D$  is the diffusion coefficient ( $\text{cm}^2 \text{s}^{-1}$ ),  $A$  is the geometric area (approximate substitution of real area) of the electrode ( $\text{cm}^2$ ),  $c$  is the concentration of methanol ( $\text{mol cm}^{-3}$ ) and  $n$  is the total number

of electrons transfer in the oxidation of methanol. Using the slope of  $I_{\text{net}}$  versus  $t^{-1/2}$  relationship, the value of  $D$  is calculated to be  $1.28 \times 10^{-8} \text{ cm}^2 \cdot \text{s}^{-1}$ . Figure 6C displays  $I_{\text{cat}}/I_L$  is linear proportional to the square root of time. When the oxidation current is dominated by the rate of electrocatalytic reaction of methanol, the relationship of  $I_{\text{cat}}/I_L$  with respect to  $t^{1/2}$  can be written as follows [55]:

$$\frac{I_{\text{cat}}}{I_L} = \pi^{1/2} (k_{\text{cat}} ct)^{1/2}$$

where  $I_{\text{cat}}$  and  $I_L$  are the catalytic currents in the presence of methanol and the limit current in the absence of methanol respectively.  $k_{\text{cat}}$ ,  $c_0$  and  $t$  are respectively the catalytic rate constant ( $\text{cm}^3 \cdot \text{mol}^{-1} \cdot \text{s}^{-1}$ ), concentration of methanol ( $\text{mol} \cdot \text{cm}^{-3}$ ) and time elapsed (s). From the slope of  $I_{\text{cat}}/I_L$  with respect to  $t^{1/2}$ , the catalytic rate constant  $k_{\text{cat}}$  is obtained to be  $1.55 \times 10^4 \text{ cm}^3 \cdot \text{mol}^{-1} \cdot \text{s}^{-1}$  for the concentration of 0.5M methanol.

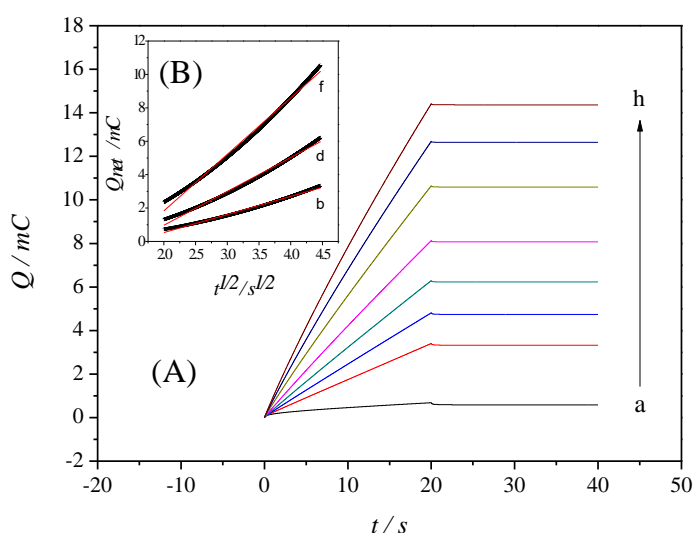


**Figure 9.** (A) Chronocoulomograms of NiMnsalpnY/GC electrode in absence (a) and presence of various concentration of methanol in the range of 0.05M-0.9M (b-h). Potential steps were 660 and 300mV, respectively. (B) Dependency of net current on  $t^{-1/2}$  for (b) 0.05M, (d) 0.2M, (f) 0.5M methanol. Pulse width: 20s.

### 3.7. Chronocoulometric studies

Chronocoulometry is also used to further verify the kinetics of electrocatalytic oxidation of methanol at the NiMnsalpnY/GC electrode. Figure 9A shows the double steps chronocoulomograms for NiMnsalpnY/GCE in the absence (a) and presence (b-h) of various concentration of methanol with applied potential steps of 660mV and 300mV, respectively.

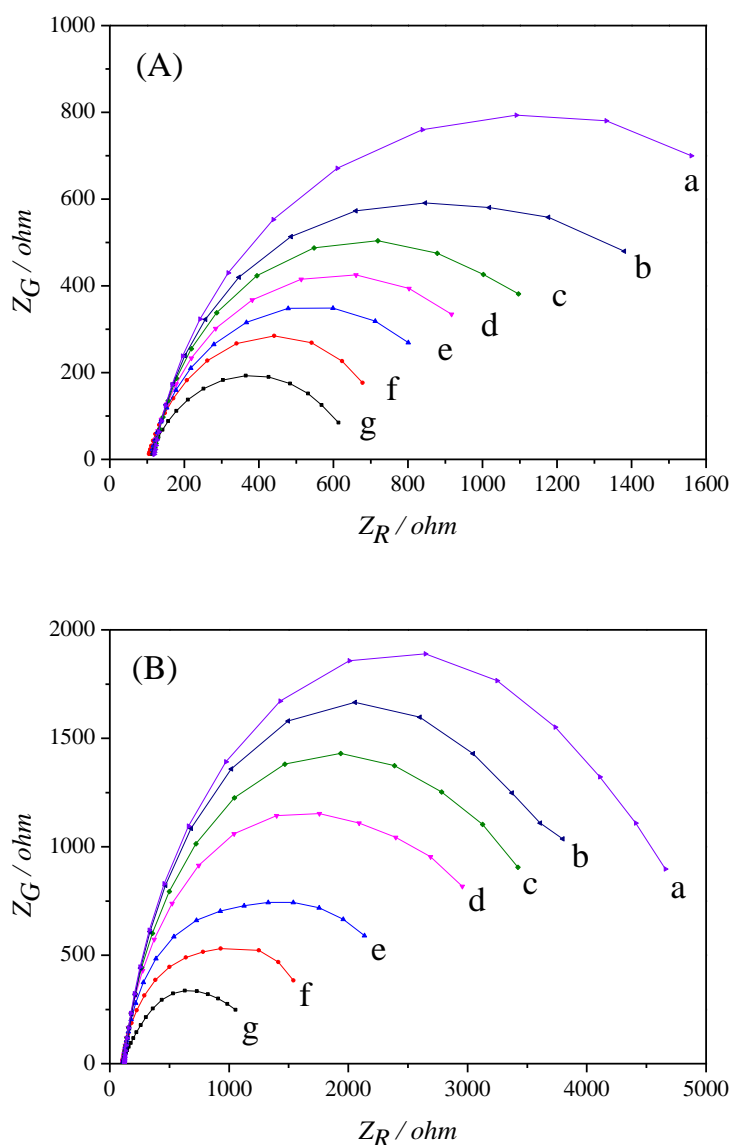


**Figure 10.** Nyquist diagrams of NiMnsalpnY/GC electrode recorded (A) at the oxidation peak potential 660mV and (B) at the low overpotential 460mV in 0.1MNaOH solution in presence of different concentration of methanol: (a) 0.05M, (b) 0.1M, (c) 0.2M, (d) 0.35M, (e) 0.5M, (f) 0.7M and (g) 0.9M.

The forward and backward potential step chronocoulometry in absence of methanol presents an almost symmetrical shape, indicating that almost equal charges are consumed for the oxidation and reduction of the surface confined Ni(III)/Ni(II) and Mn(III)/Mn(II) sites. Moreover, the large enhancement of charge and the appearance of a nearly flat line on reversal of the potential scan in the presence of methanol suggest that the electrooxidation process of methanol is irreversible [56].

Furthermore, chronocoulometry is also used to estimate the diffusion coefficient of methanol. Figure9 (B) displays that the net charge with respect to the square root of time after removing the background charge presents a linear dependency. The charge response under diffusion control is described by Cottrell equation [56]:

$$Q_{net} = 2nFAcD^{1/2}\pi^{-1/2}t^{1/2}$$

where  $D$  is the diffusion coefficient ( $\text{cm}^2\cdot\text{s}^{-1}$ ) and  $Q_{\text{net}}$  is the net charge (mC) after removing the background charge. From the slope of  $Q_{\text{net}}\cdot t^{1/2}$ , the value of  $D$  is calculated to be  $1.56\times 10^{-8}\text{ cm}^2\cdot\text{s}^{-1}$ , which is very close to the value obtained from the double step chronoamperometry.

### 3.8. Electrochemical impedance spectroscopy

In order to illuminate the resistance of the electrocatalytic oxidation system, the electrochemical impedance spectroscopy (EIS) is carried out. Figure 10A and B present the Nyquist diagrams of NiMnsalpnY/GC electrode recorded at the oxidation peak potential and the low overpotential respectively as dc-offset for various concentration of methanol (0.05M-0.9M). The Nyquist diagrams consist of two slightly depressed overlapping capacitive semicircles in the high and low frequency sides of the spectrum. The depressed semicircle corresponding to the high frequency region can be ascribed to the combined action of solution resistance, charge transfer resistance and double layer capacitance. The depressed semicircle in the low frequency region is attributed to the adsorption of the reaction intermediates and the products on the electrode surface [57].

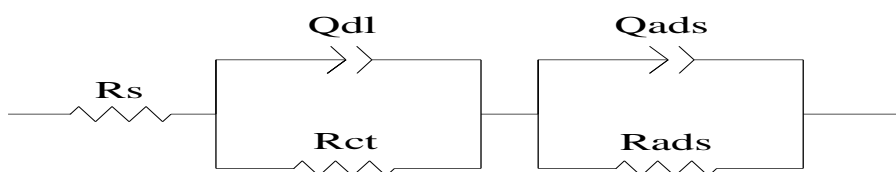


**Figure 11.** Equivalent circuit compatible with the Nyquist diagrams in Figure 8 for methanol electrooxidation at NiMnsalpnY/GC electrode.

**Table 3.**Equivalent circuit parameters fitted in the Nyquist diagrams of Figure 8A and the corresponding relative errors.

$C_{\text{methanol}}$ (M)	$R_s(\Omega)$	$R_{ct}(\Omega)$	$Q_{dl}(F)$	$Q_{ads}(F)$	$R_{ads}(\Omega)$	$n_1$	$n_2$
0.05	117.6 (1.5%)	4499 (0.96%)	0.58464(1.32%)	0.51735(1.26%)	822.7(5.13%)	0.85 (0.21%)	0.8 (0.23%)
0.1	114 (2.11%)	3346 (0.78%)	0.65119(1.53%)	0.73455(2.12%)	798.7(5.47%)	0.8 (0.31%)	0.75 (0.33%)
0.2	111.5 (1.47%)	3263 (0.43%)	0.76748(1.47%)	0.99144(2.56%)	692.7(6.62%)	0.8 (0.24%)	0.78 (0.28%)
0.35	109.4 (3.13%)	2506 (0.24%)	0.81221(1.52%)	1.04(2.84%)	472.9(5.77%)	0.82 (0.19%)	0.82 (0.21%)
0.5	96.23 (2.35%)	1145 (0.51%)	0.87516(1.61%)	1.051(2.91%)	447.5(4.93%)	0.8 (0.31%)	0.8 (0.33%)
0.7	105.3 (1.27%)	929.7 (0.76%)	0.9497(2.12%)	1.117(3.24%)	369.7(7.13%)	0.83 (0.52%)	0.81(0.43%)
0.9	105.7 (1.52%)	561.4 (0.66%)	1.008(1.45%)	1.218(3.67%)	239.8(6.28%)	0.79(0.27%)	0.75(0.32%)

**Table 4.** Equivalent circuit parameters fitted in the Nyquist diagrams of Figure 8B and the corresponding relative errors.

$C_{\text{methanol}}$ (M)	$R_s(\Omega)$	$R_{ct}(\Omega)$	$Q_{dl}(F)$	$Q_{ads}(F)$	$R_{ads}(\Omega)$	$n_1$	$n_2$
0.05	106.1 (1.2%)	1840 (0.91%)	0.75219(1.35%)	0.55856(2.11%)	1408(4.75%)	0.85 (0.13%)	0.93 (0.21%)
0.1	101 (2.26%)	1016 (0.55%)	0.78(1.46%)	0.71862(2.46%)	1324(4.86%)	0.86 (0.22%)	0.91(0.28%)
0.2	108.3 (1.56%)	867.3 (0.38%)	0.86929(1.75%)	0.99235(2.16%)	970.89(5.53%)	0.83 (0.17%)	0.93(0.33%)
0.35	113.3 (3.47%)	746.8 (0.45%)	0.87914(1.36%)	1.332(2.36%)	888.45(5.27%)	0.84 (0.16%)	0.92(0.35%)
0.5	110.5 (2.23%)	612.1 (0.62%)	0.88882(1.46%)	1.494(2.77%)	576.45(7.32%)	0.86(0.23%)	0.91(0.31%)
0.7	111.3 (1.35%)	550.2 (0.76%)	0.9713(2.41%)	1.507(2.84%)	428.9(6.27%)	0.86(0.31%)	0.94(0.38%)
0.9	116.6 (1.45%)	427.9 (0.63%)	1.007(1.84%)	1.991(2.96%)	176.6(4.96%)	0.87(0.27%)	0.96(0.29%)

The equivalent circuit compatible with the Nyquist diagram in presence of methanol is presented in Figure 11. On account of the inhomogeneous distribution caused by the microscopic roughness in the solution resistance as well as in the double-layer capacitance [57], it is necessary to replace the capacitor  $C$  with a constant phase element  $Q$  (CPE) in this equivalent circuit. Every electrical element shown in this equivalent circuit has its specific meaning.  $R_s$ ,  $R_{ct}$  and  $Q_{dl}$  signify solution resistance, charge transfer resistance and a constant phase element corresponding to the double layer capacitance.  $R_{ads}$  and  $Q_{ads}$  represent the resistance and constant phase element related to the adsorption of reaction intermediates and products. Table 3 and Table 4 show the values of equivalent circuit elements obtained by fitting the experimental results. The trueness of the fit can be judged by the estimated relative errors as presented in the parentheses. As can be seen from Table 3 and Table 4, the value of  $R_s$  corresponding to the solution resistance has not changed much, demonstrating that the increasing concentration of methanol has not had a big effect on the solution resistance.

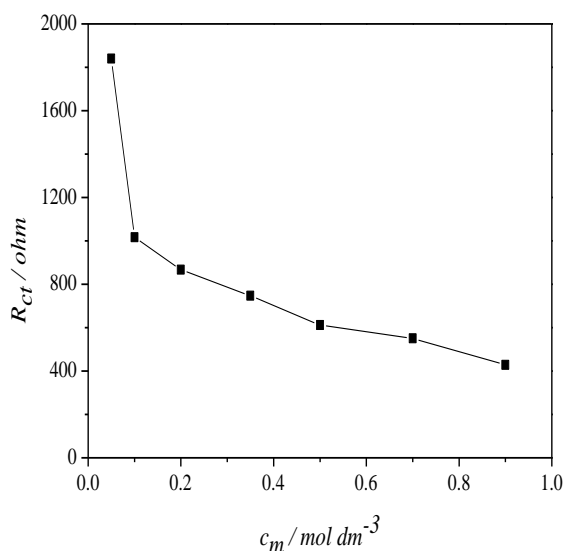


**Figure 12.** Dependency of  $R_{ct}$  on methanol concentration derived from the data of Nyquist diagrams in Figure 8B.

Moreover, with the enhancement of methanol concentration the value of  $R_{ct}$  presents a descend trend. Figure 12 shows the charge transfer resistance  $R_{ct}$  dependency on methanol concentration, where an initial sharp drop is terminated to a very slow decline as the concentration of methanol is increased above 0.2M. The charge transfer resistance of the electrode reaction has a simple physical meaning suggesting how fast charge transfer occurs on the surface of the electrode during the electrocatalytic oxidation of methanol. Based on the results, it can be concluded that a greater concentration of methanol is helpful to obtain faster charge transfer rate.

#### 4. CONCLUSIONS

In this work, the type Y zeolite composite catalyst NiMnsalpnY is synthesized by the flexible ligand method and then coated onto the glassy carbon electrodes to form a stable film. The prepared modified electrodes are tested for their electrocatalytic oxidation of methanol by the methods of cyclic voltammetry (CV), chronoamperometry (CA), chronocoulometry (CC) and electrochemical impedance spectroscopy (EIS). The experimental results of CV regime show that the NiMnsalpnY composite film has a good electrocatalytic activity towards the oxidation of methanol in alkaline solution. More specifically, the response for methanol electrooxidation at the NiMnsalpnY modified electrode is significantly larger than the response obtained for the pure Ni modified electrode. The anodic peak currents corresponding to methanol oxidation reveal a linear dependency on the square root of the scan rate, suggesting the dominance of the methanol diffusion. The mechanism of electrocatalytic oxidation of methanol based on the electrochemical cyclic regeneration of Ni(III)Mn(III) active sites and their redox reaction with methanol in subsequent process has been discussed by studying the effect of the potential scan rate and methanol concentration on the electrocatalytic current. Both the CA and CC regimes exhibit that the oxidation of methanol is an irreversible process and a diffusion controlled process. These results are in agreement with those obtained from CV regime. The kinetic parameters such as the electron transfer coefficient ( $\alpha$ ), the diffusion coefficient of methanol ( $D$ ) and the catalytic rate constant ( $k_{cat}$ ) are determined. The experimental results of the EIS regime obtained by fitting the electrical circuit compatible with the Nyquist diagrams indicate that the electrical elements in the system of methanol oxidation consist in two vital and influencing factors, namely charge transfer and adsorption.

#### ACKNOWLEDGEMENTS

This work is supported by the Natural Science Foundation for Young Scientists of Shanxi Province, China (Grant No.201701D221040), Shanxi Provincial Key Innovative Research Team in Science and Technology (No.2014131006).

#### References

1. J. Li, L. Zhao, X. Li, S. Hao, Z. Wang, *J. Electroanal. Chem.*, 40 (2020) 7.
2. A. H. Touny, *Int. J. Electrochem. Sc.*, 13 (2018) 1042.
3. W. Gong, Z. Jiang, R. Wu, Y. Liu, L. Huang, N. Hu, P. Tsiakaras, P. K. Shen, *Appl. Catal. B-Environ.*, 246 (2019) 277.
4. S. Rezaee, S. Shahrokhian, *Appl. Catal. B-Environ.*, 244 (2019) 802.
5. S.-R. Yang, S.-K. Kim, D.-H. Jung, T. Kim, H.-S. Kim, D.-H. Peck, *J. Ind. Eng. Chem.*, 66 (2018)

- 100.
6. Ó. Santiago, M. Aranda-Rosales, E. Navarro, M. A. Raso, T. J. Leo, *Int. J. Hydrogen Energy*, 44 (2019) 10933.
  7. S. S. Munjewar, S. B. Thombre, *Renew. Energy*, 138 (2019) 272.
  8. X.-Q. Hu, Q.-W. Yang, G. Xiao, X.-T. Chen, X. Qiu, *Energy Convers. Manage.*, 188 (2019) 438.
  9. W. Zheng, Y. Li, L. Y. S. Lee, *Electrochim. Acta*, 308 (2019) 9.
  10. T. Haisch, F. Kubanek, C. Haisch, D. W. Bahnemann, U. Krewer, *Electrochem. Commun.*, 102 (2019) 57.
  11. H. Wen, L.-Y. Gan, H.-B. Dai, X.-P. Wen, L.-S. Wu, H. Wu, P. Wang, *Appl. Catal. B-Environ.*, 241 (2019) 292.
  12. M. S. E. Houache, E. Cossar, S. Ntais, E. A. Baranova, *J. Power Sources*, 375 (2018) 310.
  13. X. Liu, X. Wang, J. Wu, A. Zhu, Q. Zhang, Q. Liu, *Electrochim. Acta*, 302 (2019) 145.
  14. W. Zhou, Q. Tao, J. Pan, J. Liu, J. Qian, M. He, Q. Chen, *J. Mol. Catal. A-Chem.*, 425 (2016) 255.
  15. S. Paul, S. Naimuddin, A. Ghosh, *J. Fuel Chem. Technol.*, 42 (2014) 87.
  16. W. Laosiripojana, W. Kiatkittipong, C. Sakdaronnarong, S. Assabumrungrat, N. Laosiripojana, *Renew. Energy*, 135 (2019) 1048.
  17. M. Yang, Q. Ling, R. Rao, H. Yang, Q. Zhang, H. Liu, A. Zhang, *J. Mol. Catal. A-Chem.*, 380 (2013) 61.
  18. B. Dong, W. Li, X. Huang, Z. Ali, T. Zhang, Z. Yang, Y. Hou, *Nano Energy*, 55 (2019) 37.
  19. M. Nosuhi, A. Nezamzadeh-Ejhihieh, *J. Electroanal. Chem.*, 810 (2018) 119.
  20. J. B. Raoof, N. Azizi, R. Ojani, S. Ghodrati, M. Abrishamkar, F. Chekin, *Int. J. Hydrogen Energy*, 36 (2011) 13295.
  21. A. Kawde, A. Ismail, A. R. Al-Betar, O. Muraza, *Micropor. Mesopor. Mat.*, 243 (2017) 1.
  22. A. Idris, T. A. Saleh, M. A. Sanhoob, O. Muraza, A.-R. Al-Betar, *J. Taiwan Inst. Chem. E.*, 72 (2017) 236.
  23. B. Kumar Kundu, V. Chhabra, N. Malviya, R. Ganguly, G. S. Mishra, S. Mukhopadhyay, *Micropor. Mesopor. Mat.*, 271 (2018) 100.
  24. D. R. Godhani, H. D. Nakum, D. K. Parmar, J. P. Mehta, N. C. Desai, *J. Mol. Catal. A-Chem.*, 415 (2016) 37.
  25. M. Rashvand avei, M. Jafarian, S. Etezadi, F. Gobal, M. Khakali, S. Rayati, M. Ghasem Mahjani, *Talanta*, 108 (2013) 19.
  26. J. P. Mehta, D. K. Parmar, D. R. Godhani, H. D. Nakum, N. C. Desai, *J. Mol. Catal. A-Chem.*, 421 (2016) 178.
  27. S. Pourbeyram, M. Moosavifar, V. Hasanzadeh, *J. Electroanal. Chem.*, 714-715 (2014) 19.
  28. A. Choudhary, B. Das, S. Ray, *Inorg. Chim. Acta*, 462 (2017) 256.
  29. W. Wang, R. Li, R. Zhang, J. Ma, B. Wang, *J. Electroanal. Chem.*, 742 (2015) 110.
  30. M. R. Maurya, A. K. Chandrakar, S. Chand, *J. Mol. Catal. A-Chem.*, 274 (2007) 192.
  31. K. O. Xavier, J. Chacko, K. K. Mohammed Yusuff, *Appl. Catal. A-Gen.*, 258 (2004) 251.
  32. T. M. Salama, A. H. Ahmed, Z. M. El-Bahy, *Micropor. Mesopor. Mat.*, 89 (2006) 251.
  33. K. X. Lee, J. A. Valla, *Appl. Catal. B-Environ.*, 201 (2017) 359.
  34. C. S. Martin, C. Gouveia-Caridade, F. N. Crespilho, C. J. L. Constantino, C. M. A. Brett, *Electrochim. Acta*, 178 (2015) 80.
  35. M. Keyvanfard, M. Hatami, V. K. Gupta, S. Agarwal, H. Sadeghifar, M. A. Khalilzadeh, *J. Mol. Liq.*, 230 (2017) 290.
  36. W. Yang, X. Yang, J. Jia, C. Hou, H. Gao, Y. Mao, C. Wang, J. Lin, X. Luo, *Appl. Catal. B-Environ.*, 244 (2019) 1096.
  37. H. Mao, Z. Cao, X. Guo, M. Liu, D. Sun, Z. Sun, H. Ge, Y. Zhang, X.-M. Song, *Appl. Surf. Sci.*, 471 (2019) 355.
  38. I. Danaee, M. Jafarian, A. Mirzapoor, F. Gobal, M. G. Mahjani, *Electrochim. Acta*, 55 (2010) 2093.
  39. C. L. Chiang, K. S. Lin, S. H. Yu, *J. Taiwan Inst. Chem. E.*, 98 (2019) 132.

40. S. N. Azizi, S. Ghasemi, N. S. Gilani, *Chinese J. Catal.*, 35 (2014) 383.
41. W. Zayani, S. Azizi, K. S. El-Nasser, Y. Ben Belgacem, I. O. Ali, N. Fenineche, H. Mathlouthi, *Int. J. Hydrogen Energy*, 44 (2019) 11303.
42. L. Naderi, S. Shahrokhian, *J. colloid interf. sci.*, 542 (2019) 325.
43. N. A. M. Barakat, M. Motlak, B.-S. Kim, A. G. El-Deen, S. S. Al-Deyab, A. M. Hamza, *J. Mol. Catal. A-Chem.*, 394 (2014) 177.
44. Y. Wang, D. Zhang, W. Peng, L. Liu, M. Li, *Electrochim. Acta*, 56 (2011) 5754.
45. I. Danaee, M. Jafarian, F. Forouzandeh, F. Gobal, M. G. Mahjani, *Int. J. Hydrogen Energy*, 33 (2008) 4367.
46. M. Asgari, M. G. Maragheh, R. Davarkhah, E. Lohrasbi, A. N. Golikand, *Electrochim. Acta*, 59 (2012) 284.
47. L.-S. Yuan, Y.-X. Zheng, M.-L. Jia, S.-J. Zhang, X.-L. Wang, C. Peng, *Electrochim. Acta*, 154 (2015) 54.
48. Z. Deng, Q. Yi, Y. Zhang, H. Nie, *J. Electroanal. Chem.*, 803 (2017) 95.
49. M. Motlak, N. A. M. Barakat, A. G. El-Deen, A. M. Hamza, M. Obaid, O. B. Yang, M. S. Akhtar, K. A. Khalil, *Appl. Catal. A-Gen.*, 501 (2015) 41.
50. M. Yu, S. Wang, J. Hu, Z. Chen, Y. Bai, L. Wu, J. Chen, X. Weng, *Electrochim. Acta*, 145 (2014) 300.
51. I. Danaee, M. Jafarian, F. Forouzandeh, F. Gobal, M. G. Mahjani, *Electrochim. Acta*, 53 (2008) 6602.
52. S. H. Kazemi, B. Hosseinzadeh, S. Zakavi, *Sensor. Actuat. B-Chem.*, 210 (2015) 343.
53. L. Zheng, J.-f. Song, *Talanta*, 79 (2009) 319.
54. S. Palaniappan, Y.-T. Chang, C.-M. Liu, P. Manisankar, *Mater. Chem. Phys.*, 129 (2011) 948.
55. A. Benvidi, M. T. Ghanbarzadeh, M. Mazloun-Ardakani, R. Vafazadeh, *Chinese Chem. Lett.*, 22 (2011) 1087.
56. R. Zhang, J. Ma, W. Wang, B. Wang, R. Li, *J. Electroanal. Chem.*, 643 (2010) 31.
57. P. Xie, X. Cao, Z. Lin, N. Talukder, S. Emaminejad, M. Javanmard, *Sensor. Actuat. B-Chem.*, 241 (2017) 672.